

Effect of Methoxy Substituents on the Structural and Electronic Properties of Fluorinated Cyclobutenes: A Study of Hexafluorocyclobutene and Its Vinyl Methoxy Derivatives by XRD and Periodic DFT Calculations

Leonardo Lo Presti,^{*,†} Arkady Ellern,[‡] Riccardo Destro,[†] and Bruno Lunelli[§]

Dipartimento di Chimica Fisica ed Elettrochimica, Università di Milano, Via Golgi 19, 20133 Milano, Italy, Chemistry Department, Iowa State University, 1711 Gilman Hall, Ames, Iowa 50011, and Istituto per lo Studio dei Materiali Nanostrutturati (ISMN) CNR, Via P.Gobetti, 101, 40129 Bologna, Italy

Received: September 24, 2008; Revised Manuscript Received: January 27, 2009

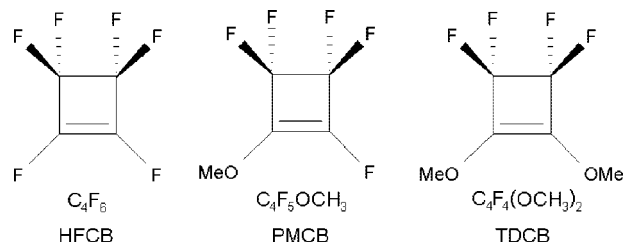
The effect of the methoxy substituent on the structure, crystal packing, and electrostatic properties of hexafluorocyclobutene (C_4F_6) was investigated in the solid-state with DFT-B3LYP calculations. Full geometry optimizations were done for the parent compound and its two vinyl methoxy derivatives $C_4F_5OCH_3$ and $C_4F_4(OCH_3)_2$, starting from the structures obtained by single-crystal X-ray diffraction at low temperature. A full topological analysis, followed by the calculation of several electrostatic properties, was performed on the periodic electron density using the quantum theory of atoms in molecules. Eventually, the cohesive energies of the three crystals were estimated. In the cyclobutene plane, the methoxy substitution yields a significant electronic rearrangement involving the π -electrons. The solid-state (periodic) results agree with those obtained by gas-phase calculations on C_4F_6 and its derivatives at a comparable level of theory. It was found that the substitution of one or two vinylic fluorine atoms with the OCH_3 group considerably influences the molecular dipole moment, which undergoes an enhancement in both the solid and the gas phase as large as 200% and 235% for $C_4F_5OCH_3$ and $C_4F_4(OCH_3)_2$, respectively, with respect to that calculated for C_4F_6 . The charge rearrangement due to the substituents provides a significant electrostatic contribution to the lattice energy, and in turn it can be related to the change in the observed crystal packing on going from C_4F_6 (space group $P2_1/c$) to both of its derivatives (space group $P\bar{1}$). It is also shown that the dispersion energy significantly contributes to the lattice stability in all three compounds. Since the DFT calculations, in the limit of large separations, entirely miss the dispersion term, this was estimated by applying a recently proposed dampening function to the semiempirical atom–atom $C_6 R^{-6}$ potentials in the mainframe of Spackman's energy decomposition scheme for Mulliken multipoles.

1. Introduction

Due to their chemical inertness, hydrophobicity, and high thermal stability, fluorocarbons are attractive materials for industrial and chemical applications.¹ In the last years, several fluorinated molecules claimed a great deal of attention also in pharmaceutical studies, as they display significant bioisosterism² with respect to substances of biochemical interest. As an example, the fluorovinyl group ($C=C-F$) has been shown to mimic the geometry of the peptide bond,³ and it finds application in the inhibition of the enzyme dipeptidyl peptidase IV.⁴

Hexafluorocyclobutene (C_4F_6 , hereinafter HFCB; see Scheme 1) is a highly toxic olefin⁵ that is gaseous at room temperature (bp 5 °C). It is used as a heat transfer fluid in refrigeration systems⁶ or as an etching agent in the production of semiconductor devices.^{7,8} In the last decades it was studied in order to investigate the structural effects accompanying the introduction of fluorine atoms into simple hydrocarbon rings.^{9–13} The debate concerned mainly the C–C distance of the single bond opposite to the C=C double bond, because such distance was found to be larger when determined by gas-phase electron diffraction¹⁴ (GED) than when obtained by microwave spectroscopy¹⁵ (MW).

SCHEME 1: Chemical Formulae



Among other cyclobutene derivatives with various degrees of fluorination, HFCB was extensively investigated by means of theoretical methods, some of them employing very large basis sets and accurate Hamiltonians.^{10–12} The computational work of Császár¹⁰ asserted the resolution of the observed geometric discrepancies between MW and GED results in favor of the MW structure.

It is worth noting that even the ground-state geometries (not to mention transition states) are often determined by subtle electronic effects, not always simple to rationalize. As solid-state investigations, by means of single-crystal X-ray diffraction (XRD) analysis and periodic calculations, can supply accurate geometric and electronic data, they can shed more light on the effects due to substituents on the observed properties of the above-mentioned systems.

* To whom correspondence should be addressed. E-mail: leonardo.lopresti@unimi.it.

[†] Università di Milano.

[‡] Iowa State University.

[§] Istituto per lo Studio dei Materiali Nanostrutturati (ISMN) CNR.

Probably because of the difficulty in growing single crystals from substances that are liquids at standard ambient conditions ($T = 298.15$ K, $p = 1$ bar), until now HFCB has never been studied in a condensed phase. In the present work, a full XRD structure determination has been performed at low T on HFCB and its two vinyl methoxy derivatives (hereinafter PMCB and TDCB; see Scheme 1). All three diffraction experiments provided reliable information on molecular geometry and crystal symmetry that were used as a valuable starting point for solid-state geometry optimizations.

It should be stressed that for small and neutral molecules such as fluorinated cyclobutenes, the effect of crystallization on the geometry of the four-membered ring is expected to be hardly significant (if any). So, the electronic rearrangements observed on going from HFCB to its methoxy derivatives should be solely and directly related, to a good approximation, to the effect on the molecular electron density of the replacement of F atoms with OCH_3 substituents. To support this expectation, also gas-phase geometry optimizations were performed for all three compounds, and the results were compared with those of the solid phases.

As described in detail in the following section 3, after geometry optimizations, an exhaustive analysis was performed of the full total electron density and its Laplacian for all three compounds. The intramolecular and intermolecular chemical bonds were analyzed by means of the quantum theory of atoms in molecules (QTAIM),¹⁶ which is nowadays considered the most complete density-based topological tool for chemical bonding studies.¹⁷ The results of the evaluation of the electrostatic properties, including the molecular electric moments, the electrostatic potential $\varphi(\mathbf{r})$, and their contributions to the crystal cohesive energy for the three substances, are reported and compared.

2. Experimental Section

HFCB was purchased from SCM Specialty Chemicals, Gainesville, FL, and fractionally distilled, keeping the central fraction; PMCB and TDCB were prepared and purified by reported methods.^{18,19} The Lindemann glass capillaries (diameter 0.5 mm) with frozen HFCB, PMCB, and TDCB were vacuumed and sealed using a needle-sharp oxygen–hydrogen torch. In situ crystallization and further X-ray structure determination were carried out with a goniometer head mounted on a BRUKER SMART 1000TM CCD diffractometer (Mo $K\alpha$ radiation, graphite monochromator, ϕ -scan, 0.3° frame width). The crystallization, performed by slow cooling, started at a temperature slightly above the melting point of each sample. Other details of the procedure are available in the Supporting Information. A standard crystallization experiment usually takes 5–6 h while the process is monitored by inspecting the diffraction frames. Unfortunately, several attempts to obtain true single crystals of HFCB, PMCB, and TDCB always led to many crystallites; therefore, the diffraction data were collected using a full sphere algorithm and the further structure determinations were performed by treating each crystal as a multitwin sample. For each substance, in spite of the coexistence of many (5–15) crystallites, it was always possible to isolate a set of reflections ascribable to one and only one crystalline individual, i.e. without overlaps between F_{hkl} belonging to different lattices. This independent data set was carefully isolated from the entire multitwin diffraction pattern by means of a visual procedure with the RLATT software.²⁰ The three structures were successfully solved by the direct methods and subsequently refined by the SHELXTL²¹ program package. The thermal motion of all

the non-hydrogen atoms was treated by the full-matrix anisotropic approximation. The final parameters²² were used as a starting point for full periodic geometry optimizations, as described in the next section.

3. Computational Details

3.1. Geometry Optimizations. For all three compounds, the XRD atomic coordinates were fully relaxed in the solid-state by using the automated routine provided in the 2003 version of the CRYSTAL code.²³ The same standard 6-31G(d)^{24,25} basis set at the DFT-B3LYP^{26,27} level of theory was adopted in all the calculations. Because of the high computational time required for the optimization of the two low-symmetry derivatives, a more sophisticated approach was considered not feasible. Cell parameters and crystal symmetries were kept fixed during the whole optimization process to those provided by the XRD experiments. For both PMCB and TDCB, serious convergence problems were detected when all the atom positions were allowed to be simultaneously optimized using the experimental geometry as starting point. Full details concerning the refinement method as well as details of the adopted strategy for a successful refinement and on the computer time required by the whole process are reported in the Supporting Information.

It is worth noting that a full frequency analysis in the solid state should be performed to ensure that a true minimum of the potential energy surface (PES) has been effectively reached. At the same time, it should be observed that in the present case such calculations are very demanding, since in all the three derivatives the asymmetric unit always coincides with the whole molecule. Therefore, the symmetry cannot be used to simplify and speed up the evaluation of the mass-weighted dynamical matrix. Moreover, both PMCB and TDCB crystallize in the space group $P\bar{1}$, so for these two substances, it is not possible to reduce the number of k points in the first Brillouin zone, where the SCF procedure has to be applied to solve the Kohn–Sham equations. We estimate that a full frequency analysis would require about 1 month per compound, being at the same time far beyond the scope of the present work. Anyhow, the following points are worth note: (i) all the final geometries in the solid-state are fully consistent with those obtained from the experimental methods (XRD, MW, and GED); (ii) all the compounds were optimized starting from accurate XRD positional parameters; (iii) very tight tolerances were adopted on energy eigenvalues between consecutive cycles in the SCF iteration and on the evaluation of the Coulomb and exchange series (see the Supporting Information), so the corresponding SCF energies are very accurate. For all these reasons, it is truly unlikely that the stationary points on the PES are not in fact true minima. To provide a firmer ground to this assertion, the frequencies at the optimized gas-phase geometries of all the three derivatives were also evaluated using the Gaussian 03 program²⁸ (vide infra). No negative or somewhat unrealistic vibration frequencies were found. These results cannot be used, of course, to prove unequivocally that the same is true in the condensed phase; anyway, since there are only minor differences between the molecular geometries in the gas-phase and in the bulk (see section 4.1), it reinforces our guess that we are dealing with sensible minima even in the solid-state.²⁹

Gas-phase calculations were also performed for all three compounds using Gaussian 03²⁸ with the 6-311+G(d) basis set³⁰ and the DFT-B3LYP^{26,27} Hamiltonian. For each of the isolated molecules, the corresponding atomic positions were both allowed to relax and kept fixed to their optimized periodic

TABLE 1: Symmetry and Crystal Data for HFCB, PMCB, and TDCB

	HFCB	PMCB	TDCB
	General Information		
chemical formula	C ₄ F ₆	C ₄ F ₅ OCH ₃	C ₄ F ₄ (OCH ₃) ₂
chemical name	hexafluorocyclobutene	1,3,3,4,4-pentafluoro-2-methoxycyclobutene	3,3,4,4-tetrafluoro-1,2-dimethoxycyclobutene
molecular weight (amu)	162.04	174.08	186.11
melting point (°C) ^a	-60	-42	-0.5 to 0 ^b
	Crystal Information		
data collection <i>T</i> (K)	178(2)	193(2)	193(2)
space group	<i>P</i> 2 ₁ / <i>c</i>	<i>P</i> 1̄	<i>P</i> 1̄
<i>a</i> (Å)	6.026(2)	5.999(5)	7.271(7)
<i>b</i> (Å)	11.035(3)	7.029(7)	7.590(7)
<i>c</i> (Å)	7.849(2)	8.307(8)	7.729(7)
α (deg)	90.0	73.708(16)	73.415(15)
β (deg)	71.370(4)	71.854(16)	94.823(17)
γ (deg)	90.0	74.380(20)	68.702(15)
cell volume (Å ³)	494.6(3)	313.1(5)	372.4(6)
calculated density (g cm ⁻³)	2.176	1.847	1.660
<i>Z</i>	4	2	2

^a Melting points have been taken from <http://www.chemicalbook.com/indexEN.aspx> ^b Also reported as -5.3 °C in ref 61.

values, in order (i) to estimate the molecular relaxation energies (vide infra) and (ii) to compare the gas-phase and the solid-state geometries.³¹

3.2. Topological Analysis of the Electron Density. After convergence was achieved, for all three substances a single-point calculation on the final geometry was performed with the CRYSTAL98 version³² of the code, employing the same basis set, Hamiltonian, and computational parameters (as described in the Supporting Information). The topology of the resulting electron density was then analyzed for both the intramolecular and the intermolecular interactions with the TOPOND98 code³³ and the integration quality over the zero-flux surfaces of each atomic basin¹⁶ was checked by means of the integrated Lagrangian, which was on average as low as 0.0005 e Å⁻² for HFCB, 0.0004 e Å⁻² for PMCB, and 0.0010 e Å⁻² for TDCB, respectively. None of the three substances showed appreciable residual charge³⁴ on the asymmetric unit after the integration, the maximum residual being 0.004 *e* for TDCB; moreover, the experimental cell volumes were all retrieved within 0.75 Å³ by summing the individual atomic volumes.

3.3. Cohesive Energies. The cohesive energy of each of the three molecular crystals was evaluated as

$$E_{\text{cohesive}} = E_{\text{bulk}}/Z - E_{\text{iso}} - E_{\text{rel}} + E_{\text{BSSE}} \quad (1)$$

as recently described in this journal.³⁵ Here E_{bulk} is the total energy of the unit cell, Z is the number of formula units in each cell, E_{iso} is the energy of an isolated molecule which keeps its solid-state conformation, E_{rel} is the relaxation energy (it is a negative term accounting for the difference between the energies of an isolated molecule in its bulk and gas-phase conformations³⁵), and E_{BSSE} is the correction due to the basis set superposition error (BSSE).

In order to reduce the amount of the BSSE, single-point calculations corresponding to the final solid-state optimized geometry were performed with the DZ (Dunning)^{25,36} basis set. All the energies were corrected by the counterpoise method (CP).³⁷ CRYSTAL03²³ applies the CP method by supplementing the molecular basis set with the basis functions of an increasing number of “ghost” atoms, placed at the crystallographic atomic positions within a certain distance from the reference molecule. In this work, all the “ghosts” within 5.0 Å were considered,

including up to 86 neighbors for HFCB, 115 for PMCB, and 123 for TDCB.

E_{rel} was evaluated by means of Gaussian 03²⁸ calculations on the isolated molecules using the 6-311+G(d) basis set³⁰ with the DFT-B3LYP^{26,27} Hamiltonian, without imposing symmetry constraints on the molecular unit. The greatest correction due to the relaxation energy was detected in PMCB and amounted to -1.71 kJ mol⁻¹.

It should be kept in mind that this model for the crystal cohesive energy cannot be directly related to thermodynamic quantities such as the standard sublimation enthalpies at 0 K, $\Delta_{\text{sub}}H^{\circ}(0)$, because it lacks two important contributions: the vibrational zero-point energy of the molecules in the crystalline state and the dispersion (van der Waals) energy³⁸ at large separations. In particular, the latter term is known to be entirely missed by ground-state DFT methods,³⁹ because they cannot account for correlations between distant electrons when these differ from those of a uniform (or near-uniform) electron gas.

To properly estimate the dispersion term, the Spackman's E_{cryst} energy partition model⁴⁰⁻⁴⁴ as implemented in PAMOC⁴⁵ was applied to an expansion of atom-centered Mulliken spherical-harmonic multipoles up to $l = 4$. The dispersion E_{dis} contribution was approximated by an R^{-6} atom-atom potential, which was dampened according to Grimme⁴⁶ with an inverse exponential function to avoid singularities at small R . More details about the E_{cryst} approach as it was applied in the present work are available in the Supporting Information.

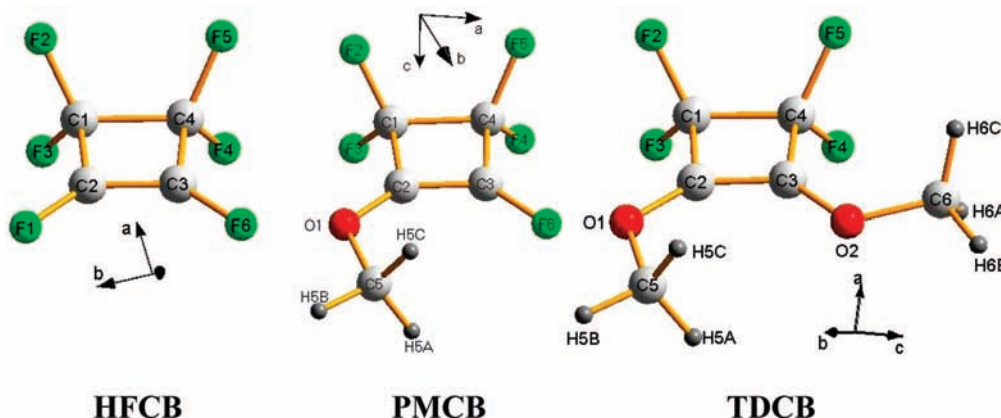
4. Results and Discussion

The structural results of the periodic DFT-B3LYP geometry optimizations for HFCB, PMCB, and TDCB are collected in Table 2 (see Scheme 2 for the atom numbering sequence). In the Supporting Information we report a brief comparison of geometry optimization results for HFCB in the solid state with those of ref 10 on the isolated molecule. In the following, we first discuss some considerable features of the molecular geometries and then report on the topological analysis of the electron density, to explain some of the observed trends in bond distances and angles. Subsequently, the effects of the electron-releasing methoxy substitution on the crystal packing and some physical properties (mainly molecular dipole moments) are examined. Finally, a discussion on the calculated crystal energies is presented.

TABLE 2: Optimized Geometries of HFCB, PMCB, and TDCB in the Solid-State Compared with Other Theoretical and Experimental Values

distances (Å) and angles (deg) ^a	HFCB, C ₄ F ₆						PMCB, C ₄ F ₅ OCH ₃			TDCB, C ₄ F ₄ (OCH ₃) ₂		
	GP opt		X-ray ^e	GED ^f	MW ^g	P opt	GP opt present work	X-ray	P opt	GP opt present work	X-ray	
	P opt ^b	ref 12 ^c										present work ^d
C1–C4	1.5690	1.5618	1.5768	1.559 (4)	1.583 (5)	1.552 (3)	1.5606	1.5710	1.545 (4)	1.5518	1.5594	1.545 (11)
C1–C2	1.5038	1.4962	1.5018	1.482 (5)	1.501 (3)	1.478 (3)	1.5049	1.5067	1.483 (3)	1.4907	1.4940	1.468 (11)
C2=C3	1.3428	1.3374	1.3374	1.322 (4)	1.326 (11)	1.333 (3)	1.3562	1.3498	1.336 (4)	1.3643	1.3587	1.340 (9)
C3–C4	1.5041	1.4962	1.5018	1.486 (4)	1.501 (3)	1.478 (3)	1.4889	1.4896	1.455 (3)	1.5015	1.4981	1.480 (11)
C1–F2	1.3564	1.3402	1.3523	1.346 (3)	1.347 (3)	1.358 (<1) ^h	1.3608	1.3559	1.353 (4)	1.3636	1.3625	1.370 (8)
C1–F3	1.3595	1.3402	1.3534	1.343 (3)	1.347 (3)	1.358 (<1) ^h	1.3652	1.3559	1.356 (3)	1.3723	1.3625	1.351 (6)
C4–F4	1.3549	1.3402	1.3523	1.346 (3)	1.347 (3)	1.358 (<1) ^h	1.3650	1.3591	1.359 (4)	1.3667	1.3681	1.344 (8)
C4–F5	1.3583	1.3402	1.3532	1.347 (3)	1.347 (3)	1.358 (<1) ^h	1.3652	1.3591	1.350 (3)	1.3733	1.3684	1.361 (8)
C2–X1 ⁱ	1.3141	1.3058	1.3105	1.309 (3)	1.313 (5)	1.309 (2) ^h	1.3131	1.3165	1.315 (3)	1.3277	1.3260	1.341 (10)
C3–X2 ^j	1.3152	1.3058	1.3106	1.309 (4)	1.313 (5)	1.309 (2) ^h	1.3294	1.3271	1.330 (3)	1.3349	1.3378	1.342 (8)
C4–C1–C2	85.75	85.70	85.43	85.4 (2)	85.1 (3)	85.7 (1)	86.84	86.53	86.5 (2)	86.51	86.11	85.8 (5)
C3=C2–C1	94.25	94.30	94.57	94.8 (2)	94.9 (3)	94.3 (1)	92.36	92.62	92.3 (2)	93.89	94.07	94.8 (6)
C2=C3–C4	94.37	94.30	94.57	94.3 (2)	94.9 (3)	94.3 (1)	95.47	95.86	95.9 (2)	93.25	93.63	93.1 (6)
C3–C4–C1	85.63	85.70	85.43	85.5 (2)	85.1 (3)	85.7 (1)	85.30	84.99	85.4 (2)	86.27	86.20	86.3 (6)
F2–C1–F3	107.63	107.92	107.37	107.1 (2)	107.6 (3)	105.99 (<1) ^h	106.80	107.14	105.7 (2)	105.87	106.23	105.3 (5)
F4–C4–F5	107.60	107.92	107.39	107.2 (2)	107.6 (3)	105.99 (<1) ^h	106.12	106.51	105.7 (2)	105.81	105.58	105.3 (6)
C3=C2–X1 ⁱ	134.90	135.16	134.87	134.9 (3)	135.3 (6)	134.5 (1) ^h	139.37	140.08	140.3 (2)	139.58	139.20	139.5 (7)
C2=C3–X2 ^j	134.96	135.16	134.89	135.6 (3)	135.3 (6)	134.5 (1) ^h	133.54	134.37	133.8 (2)	133.29	133.35	134.1 (8)
C1–C2–X1 ⁱ	130.85	130.54	130.55	130.3 (2)	129.8 (7)	131.2 (1)	128.27	127.31	127.4 (2)	126.52	126.74	125.6 (6)
C4–C3–X2 ^j	130.66	130.54	130.54	130.0 (3)	129.8 (7)	131.2 (1)	130.98	129.77	130.3 (2)	133.43	133.02	132.8 (7)

^a Estimated standard deviations (esd's) are in parentheses. See Scheme 2 for the atom numbering sequence. ^b This work: periodic DFT B3LYP optimization with the 6-31G(d) basis set (in bold). The molecule has C_1 symmetry. ^c Gas-phase CCSD(T) optimization with cc-pVTZ basis set, from ref 10. ^d This work: gas-phase DFT B3LYP optimization with 6-311+G(d) basis set. The molecule has C_1 symmetry. ^e This work: conventional refinement against single crystal XRD data (see the text), with no correction for thermal motion. The molecule has C_1 symmetry. ^f Experimental gas-phase electron diffraction results, from ref 14. The molecule was assumed to have C_{2v} symmetry. ^g Experimental gas-phase microwave spectroscopy results, from ref 15. The molecule was assumed to have C_{2v} symmetry. ^h Average of columns 3 and 4 in Table 4 of ref 15. ⁱ X1 = F1 in HFCB and X1 = O1 in both PMCB and TDCB. ^j X2 = F6 in both HFCB and PMCB, but X2 = O2 in TDCB.

SCHEME 2: Atom Numbering Scheme^a

^a Ball-and-stick pictures created by Diamond v3.1f (Brandenburg, K. *Diamond-Crystal and Molecular Structure Visualization*; Crystal Impact GbR: Bonn, Germany, 2008; <http://www.crystalimpact.com/diamond/>).

4.1. Effect of the Crystallization on the Geometric Parameters of the Asymmetric Unit. The gas-phase optimizations of the three substances performed with the 6-311+G(d) basis set (see the Computational Details above) allowed us to qualitatively estimate the influence of the crystal packing on the molecular geometry. In general, the effect of crystallization on the bond distances is barely significant. As an example, for the four covalent bonds in the cyclobutene ring, the quantity $\langle |d_p - d_g| \rangle$ (d_p and d_g being the covalent bond lengths in the optimized solid-state and gas-phase geometries, respectively) comes out as low as 0.0044(28) Å for HFCB, 0.0048(45) Å for PMCB, and 0.0050(20) Å for TDCB (mean standard deviations are in parentheses; see also Table 2). Interestingly, the optimized C–H distances in the methyl groups are substantially unchanged upon crystallization, with $\langle |d_p - d_g| \rangle = 0.0010(9)$ Å in PMCB and 0.0011(7) Å in TDCB. In all three substances, the solid-

state bond angles within the four-membered ring are identical within 0.4° to the corresponding gas-phase values, whereas more significant differences emerge when the angles involving H atoms are compared. As an example, in PMCB the H5B–C5–O1 bond angle value is 109.873° in the solid-state and 110.216° in the optimized gas-phase geometry. The same value for the angle is 109.538° (solid-state) and 110.400° (gas phase) in TDCB. Clearly, the crystal field mainly affects the conformation of the exocyclic methoxy groups, with a minor influence on the cyclobutene ring.

4.2. Geometry Changes in the Asymmetric Unit Due to Substituents. All the methoxy groups added in vinylic positions in the PMCB and TDCB compounds adopt a planar geometry, lying in the main molecular plane with dihedral angles of 179.93° and 179.86° for the atom sequence C5–O1–C2–C1 in PMCB and TDCB, respectively, and of –179.72° for

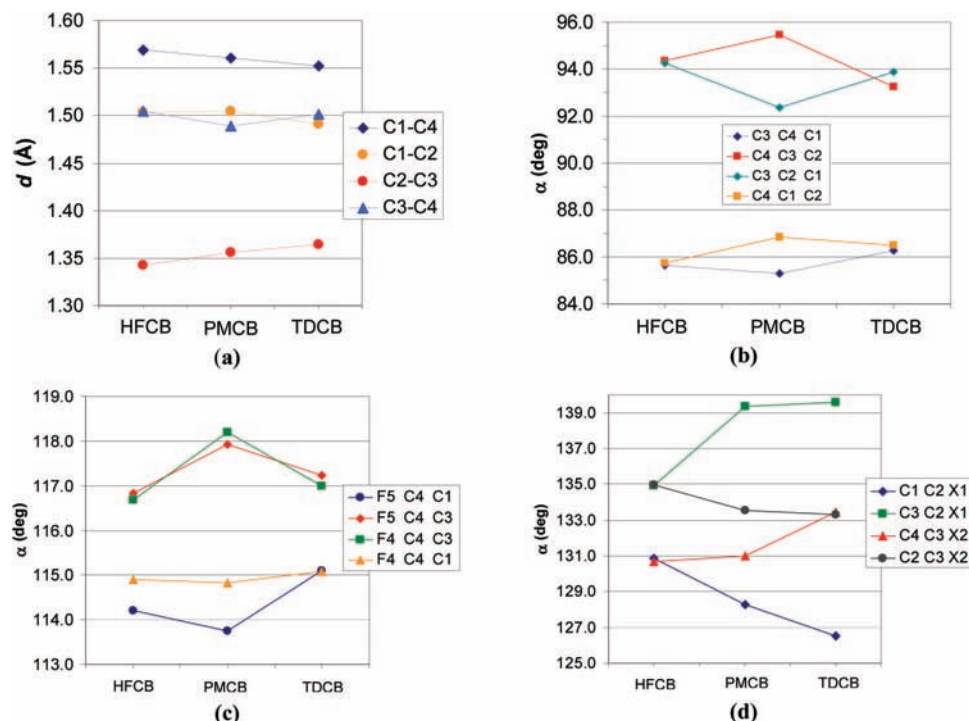


Figure 1. Changes in selected geometrical parameters in the cyclobutene ring of HFCB, PMCB, and TDCB depending on the methoxy substitution degree: (a) covalent bond distances, (b) covalent bond angles, (c) F–C–C angles at one of the sp^3 corners of the ring, and (d) vinyl bond angles. X1 = F1 in HFCB, but X1 = O1 in both PMCB and TDCB; X2 = F6 in both HFCB and PMCB, but X2 = O2 in DPMCB.

C6–O2–C3=C2 in TDCB (see Scheme 2 for the atom numbering sequence). Consequently, the distances of the methyl carbon atoms to the least-squares molecular planes defined by the cyclobutene moiety are within ± 0.08 Å: 0.037 Å for C5 in PMCB and 0.066 and -0.076 Å for C5 and C6, respectively, in TDCB.

Looking at Table 2 and Figure 1, some trends are clearly detectable. For instance, progressive substitution of equatorial fluorine atoms causes the C1–C4 bond to be linearly shortened, while the opposite C2=C3 bond is linearly lengthened. Both the C1–C2 and the C3–C4 bonds show a nonmonotonous variation in their length on going from HFCB to TDCB. The same trend becomes more perceptible when the C–C–C angles in the cyclobutene ring are considered (e.g., see the C3=C2–C1 and its complementary C4–C3=C2 angles; Figure 1b). After the second methoxy substitution, the angles in the cyclobutene ring of TDCB are only slightly distorted with respect to those observed in the parent compound, HFCB. Qualitatively, an analogous behavior is followed by the F–C–C angles at the sp^3 carbons (see Figure 1c as an example), while the F–C–F angles tend to monotonically squeeze themselves together (see Table 1). More interesting is perhaps the behavior of the angles around the vinyl carbons (see Figure 1d). In HFCB, the external angles in the four-membered ring are equal two by two, C3=C2–F1 being identical to C2=C3–F6 and C1–C2–F1 being very similar to C4–C3–F6. Asymmetries became evident in these angles when the first methoxy group is added and the O1 oxygen atom replaces the F1 atom: the angle C3=C2–O1 opens by more than 4° , while the complementary angle C2=C3–F6 tends to close itself by almost 2° . Similarly, the angle C1–C2–F1 opens and the amplitude of the angle C4–C3–F6 is reduced. When the second OCH₃ group is inserted, with atom O2 replacing atom F6, the angle C4–C3–O2 becomes equal to the angle C2=C3–O2, while the angle C3=C2–O1 turns out to be greatly different from the adjacent angle C1–C2–O1, the latter being narrower by more than 10° .

The reasons for the observed geometry changes may be investigated in terms of electronic effects, which can be rationalized by means of the topological analysis of the electron density according to Bader's quantum theory of atoms in molecules (QTAIM).¹⁶ This will be done in the next section.

4.3. Compared Topological Analysis of $\rho(\mathbf{r})$ in the Asymmetric Units of the Three Derivatives. It is well-known that the chemical bonds in molecules can be characterized through the values displayed at the corresponding bond critical points (bcp's) by such functions as the electron density $\rho(\mathbf{r})_{\text{bcp}}$, its Laplacian $\nabla^2\rho(\mathbf{r})_{\text{bcp}}$, and the Hessian eigenvalues of $\rho(\mathbf{r})_{\text{bcp}}$.¹⁶ A full list of these topological properties for all three compounds here studied (inclusive of the significant intermolecular contacts) as well as of the potential and kinetic contributions to the energy density at the bcp's of all three (as evaluated directly from the wave function) can be found in the Supporting Information (Tables S1–S5). Figure 2 reports the change in $\rho(\mathbf{r})_{\text{bcp}}$ and in the corresponding $\nabla^2\rho(\mathbf{r})_{\text{bcp}}$ as a function of the number of methoxy substituents, while Table 4 and Figure 3 show the noticeable results of the integration of the charge density contained in each atomic basin, which according to QTAIM is defined as the region bounded by a zero-flux surface in the trajectories of $\nabla\rho(\mathbf{r})$.¹⁶

The Laplacian of $\rho(\mathbf{r})$ at the C1–F1 and C3–F6 bcp's is positive (see Figure 2b), but this is not unusual for highly polar bonds.^{17,47} In fact, the bcp shifts toward the less electronegative atom and reaches the region of core charge depletion of the carbon L shell, where its closeness to the nodal $\nabla^2\rho(\mathbf{r})$ surface makes the sign of the corresponding Laplacian very sensitive to little changes in the critical point coordinates.

The behavior of bonds C1–C4 and C2=C3 is in agreement with the previously discussed variation of the bond lengths, the first covalent interaction being reinforced and the latter weakened as a consequence of the insertion of the oxygen atoms on the equatorial carbons. Substitution of F1 with the group O1–CH₃ has little effect on the remaining C–F bonds, whose

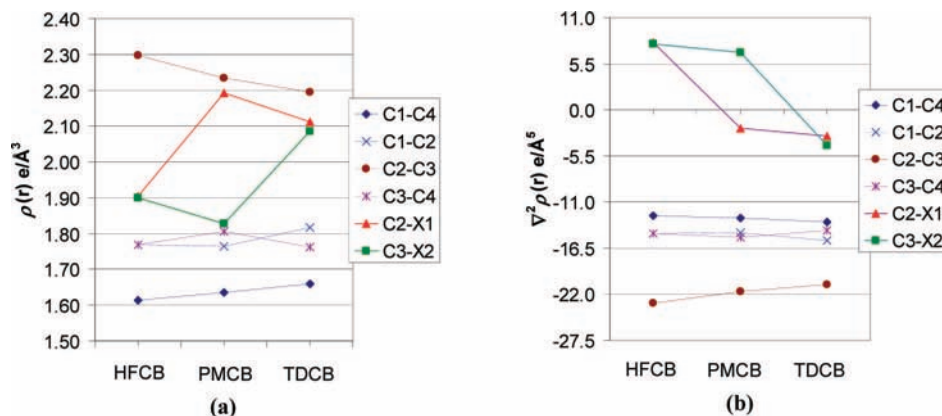


Figure 2. Changes in the topological parameters of the primary electron density of HFCB, PMCB, and TDCB depending on the methoxy substitution degree. (a) $\rho(r)$ at the covalent bond critical points and (b) $\nabla^2 \rho(r)$ at the covalent bond critical points. X1 = F1 in HFCB, but X1 = O1 in both PMCB and TDCB; X2 = F6 in both HFCB and PMCB, but X2 = O2 in TDCB.

TABLE 3: Overlap Angles between Major Bond Axis Eigenvectors of Adjacent Bonds in the Cyclobutene Plane

overlap angle (deg)	HFCB	PMCB	TDCB
C1–C2/C4–C1	89.56	89.74	89.76
C3–C4/C4–C1	89.63	88.69	88.15
C1–C2/C2=C3	0.35	0.99	1.02
C3–C4/C2=C3	0.56	1.01	1.72
C3=C2/C2–X1 ^a	86.93	1.45	0.91
C4–C2/C3–X2 ^b	88.90	0.75	2.35
C1–C2/C2–X1 ^a	86.58	1.68	0.36
C2=C3/C3–X2 ^b	89.44	1.69	0.73

^a X1 = F1 in HB, and X1 = O1 in both PMCB and TDCB. ^b X2 = F6 in both HB and PMCB, but X2 = O2 in TDCB.

TABLE 4: Atomic Net Charges of HFCB, PMCB, and TDCB As Evaluated with Mulliken and QTAIM Partitioning of the Periodic 6-31G(d) Wave Function at the Solid-State Optimized Geometry

atom	Mulliken			QTAIM		
	HFCB	PMCB	TDCB	HFCB	PMCB	TDCB
C1	0.567	0.579	0.584	1.221	1.183	1.169
C2	0.273	0.223	0.207	0.687	0.708	0.645
C3	0.269	0.259	0.227	0.682	0.623	0.624
C4	0.570	0.566	0.571	1.228	1.184	1.154
C5		–0.276	–0.283		0.421	0.431
C6			–0.287			0.431
F1	–0.239			–0.638		
F2	–0.301	–0.304	–0.307	–0.634	–0.640	–0.645
F3	–0.300	–0.303	–0.317	–0.636	–0.637	–0.644
F4	–0.297	–0.307	–0.309	–0.636	–0.643	–0.641
F5	–0.300	–0.308	–0.308	–0.635	–0.638	–0.649
F6	–0.242	–0.264		–0.639	–0.655	
O1		–0.406	–0.439		–1.105	–1.117
O2			–0.443			–1.126
H5A		0.181	0.183		0.072	0.070
H5B		0.182	0.191		0.067	0.060
H5C		0.179	0.181		0.061	0.058
H6A			0.181			0.063
H6B			0.187			0.059
H6C			0.181			0.062

distances are indeed all lengthened by less than 0.7%. The equatorial C3–F6 bond is the only exception, being lengthened by 1.1%. Moreover, its $\rho(r)_{\text{bcp}}$ value undergoes a 4% reduction from HFCB to PMCB (Figure 2a, Tables S1 and S2 in the Supporting Information), which is significant if compared with the mean reduction of 1.6% in the $\rho(r)_{\text{bcp}}$ values experienced by the axial C–F bonds. Interestingly, in TDCB, when a second oxygen is added in place of F6, both the electron density and

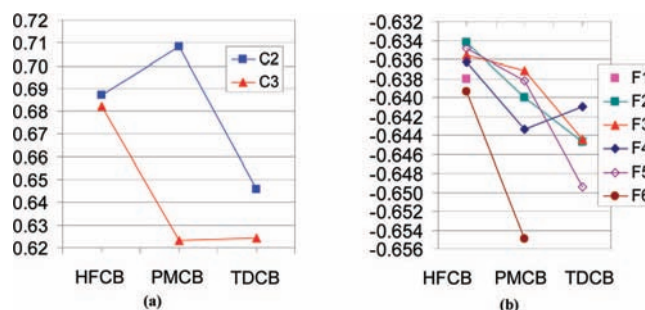


Figure 3. Bader's net charges on the vinylic carbons and on the fluorine atoms as evaluated by integration of the primary electron density within atomic basins of HFCB, PMCB, and TDCB. (a) Atomic net charges on the vinylic carbons as a function of the degree of methoxy substitution and (b) atomic net charges on the fluorines as a function of the degree of methoxy substitution.

its Laplacian at the two C2–O1 and C3–O2 bcp's turn out to be substantially equal (Figure 2a, Tables S2 and S4 in the Supporting Information).

The eigenvector associated with the λ_2 eigenvalue of the Hessian matrix of the electron density at the bcp characterizes by definition the major axis of the bond,¹⁶ determining the relative orientation within the molecule of the charge accumulation plane around the bcp itself. So, the mutual alignment of such vectors in adjacent bonds can be used to recognize conjugative or even hyperconjugative electronic effects.^{48,49} The angles between the λ_2 eigenvectors for all the covalent bonds in the main molecular plane of HFCB, PMCB, and TDCB were computed, and the results are reported in Table 3. In HFCB, the major axis of the C2=C3 bond appears to be almost perfectly aligned with those of the adjacent C2–C1 and C3–C4 bonds, but not with that of C1–C4 nor with those of the equatorial C2–F1 and C3–F6 bonds. When F1 is substituted with O1, the major C3–F6 axis rotates by roughly 85°, becoming aligned with those of all the other bonds in the plane except the C1–C4 bond. At the same time, the electronic populations of both atoms C3 and F6 increase, resulting in a lower positive charge on the carbon and in a greater negative charge on the fluorine atom (see Table 4 and Figure 3). According to the “rules” of organic chemistry, this electronic rearrangement can be rationalized by means of the electron-withdrawing ability of the equatorial F6, which attracts the charge density provided by the methoxy donor group through the delocalized π system around the C2=C3 bond. As a matter of fact, fluorine is the most electronegative atom in the periodic table, but it is also too small and hard to stabilize a great amount of negative charge, so (as an example)

it shows a lower electron affinity than the less electronegative chlorine.⁵⁰ Inspection of atomic populations (as calculated by Bader's charges) of C3 and F6 reported in Table 4 shows that in PMCB the electronic population in the fluorine basin increases only by 0.16%, whereas in the C3 basin the increment amounts to more than 1.0% with respect to HFCB. This in turn increases the Coulombic repulsion between the charge density contained in the C and F adjacent basins, and the entire electronic rearrangement results in a slightly greater C3–F6 equilibrium bond distance in PMCB with respect to that of HFCB. Interestingly, a study on several fluorinated carbenes⁵¹ shows that the C–F bond length (d_{C-F}) is greater when an alkoxy group is added to the carbene atom (e.g., $d_{C-F} = 1.353 \text{ \AA}$ in *cis*-fluoro(hydroxy)carbene at the CCSD/DZ+P theory level, whereas $d_{C-F} = 1.300 \text{ \AA}$ in difluorocarbene as obtained from microwave spectroscopy). Furthermore, we have obtained similar results when comparing the optimized gas-phase geometries of *cis*-1,2-difluoroethylene and *cis*-1-fluoro-2-methoxyethylene both at the DFT-B3LYP/6-31G(d) and at the CCSD/TZ^{25,52–54} theory levels. More in detail, d_{C-F} increases from 1.3424/1.3991 \AA in *cis*-1,2-difluoroethylene to 1.3586/1.4180 \AA in *cis*-1-fluoro-2-methoxyethylene (B3LYP/CCSD results).

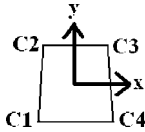
Considering the 6-311+G(d) results of the gas-phase optimized geometry, it should be stressed that also in the isolated compounds both geometrical and topological parameters of the cyclobutene ring follow exactly the same trend observed in the condensed phases. As an example, in the gas-phase $\rho(\mathbf{r})_{\text{bcp}}$ for the formally double C2=C3 bond decreases monotonically from 2.307 $e \text{ \AA}^{-3}$ (HFCB) to 2.236 $e \text{ \AA}^{-3}$ (PMCB) until 2.202 $e \text{ \AA}^{-3}$ (TDCB) as the degree of methoxy substitution is increased. At the same time, $\rho(\mathbf{r})_{\text{bcp}}$ of the C3–F6 bond undergoes a $\sim 4\%$ reduction on going from HFCB (1.872 $e \text{ \AA}^{-3}$) to PMCB (1.788 $e \text{ \AA}^{-3}$). The two C2=C3 and C3–F6 bond distances are consequently lengthened, too. So, the electronic rearrangement observed in the solid state should be considered as an effect truly induced by the methoxy substituents, as the related geometrical and topological trends are evident already in the isolated, gas-phase molecules.

In both the solid state and the gas phase, the equilibrium C–F distance in vinyl groups is therefore a matter of delicate balance between the electron conjugation effect in the main molecular plane and the increased Coulombic repulsion between the electron density contained in the C3 and F6 basins. When in TDCB the second methoxy group replaces F6, a more symmetrical charge distribution appears around the vinyl bond, in that the net charges of the C2/C3 and O1/O2 basins, as well as the electron density and its Laplacian at the corresponding bcp's, became similar to each other.

4.4. Crystal Packing of HFCB, PMCB, and TDCB: Compared Analysis on Electrostatic and Topological Grounds. Inspection of Table 1 shows that the equatorial fluorine substitution with methoxy groups has dramatic effects on both crystal packing and physical properties of the HFCB derivatives. The melting point increases monotonically on going from HFCB to TDCB, indicating that the solid phase becomes stable over a wider temperature range as the methoxy degree of substitution increases (which in turn can be related to an increase in the crystal cohesive energy; see the next section). Moreover, the crystal symmetry is reduced on going from HFCB (space group $P2_1/c$) to PMCB (space group $P\bar{1}$), whereas it is not changed when the second OCH₃ group is inserted in TDCB (space group $P\bar{1}$).

Table 5 reports the molecular dipole moments as evaluated with Bader's partitioning scheme of the electron density.⁵⁵ The mutual orientation of the dipole moments in the unit cell is

TABLE 5: Molecular Dipole Moments of HFCB, PMCB, and TDCB at the Periodic and Gas-Phase Optimized Geometries As Evaluated from Bader's Partitioning Scheme^a



	optimized periodic B3LYP/6-31G(d) geometry			optimized gas-phase B3LYP/6-311+Gd geometry		
	HFCB	PMCB	TDCB	HFCB	PMCB	TDCB
X	-0.0909	-0.6169	3.3180	-0.0544	-0.9335	2.2461
Y	1.8929	5.6852	5.3986	1.5552	4.6009	4.7217
Z	0.0313	0.2069	0.3953	-0.0216	0.0699	-0.2732
$ \mu $	1.8954	5.7223	6.3491	1.5563	4.6952	5.2358

^a All quantities are expressed as debye. Dipole components are referred to the same right-handed orthogonal Cartesian reference system (see the structure), with each molecular center of mass taken as the origin.

shown in Figure 4. All quantities are reported in units of debye; for the sake of comparison with the same quantities in the gas phase, the equivalent right-handed orthogonal reference system shown in the inlet of Table 5 was chosen for all three derivatives. For each substance, the modulus of the dipole moment increases by about 20% in the solid-state with respect to that evaluated in the isolated molecule (see Table 5). With respect to its orientation in the gas phase, the dipole vector remains substantially unchanged in HFCB (Figure 4a), while upon crystallization it rotates by $\sim 8^\circ$ and $\sim 9^\circ$ in PMCB and TDCB, respectively (Figure 4b,c).

Even for this property (μ), on going from HFCB to PMCB and TDCB the trend observed in the solid state is mirrored by that in the gas phase. The substitution of equatorial fluorine atoms with methoxy groups has important consequences on the electrostatic properties of the system. The dipole moments in both the solid and the gas state increase by as much as 202% and 235–236% on going from HFCB to PMCB and from HFCB to TDCB, respectively. All three derivatives crystallize in centric space groups, so the corresponding molecular dipoles are forced by symmetry to align themselves in head-to-tail antiparallel motifs (see Figure 4). According to classical electrostatics, in the limit of dipole large separation, this arrangement represents an efficient way to increase the attractive energy between the opposite charges and to reduce the repulsion between the charges with the same sign.

As could be expected, the electronic and nuclear rearrangement due to the methoxy substitution has a noticeable effect on the electrostatic potential $\varphi(\mathbf{r})$, too. Figure 5 shows the scalar field $\varphi(\mathbf{r})$ as evaluated directly from the wave function in the crystal in the mean cyclobutene plane. In both PMCB and TDCB, zones of negative charge concentrations as deep as -0.06 to $-0.08 e \text{ \AA}^{-1}$ appear near the oxygen atoms. In particular, in Figure 5c (TDCB) some C–H \cdots O hydrogen bonds are clearly recognizable in the cyclobutene plane (those labeled as bcp_20, bcp_22, and bcp_24 in Table S5 in the Supporting Information). No similar interactions are detectable in Figure 5b (PMCB), as in this derivative all the hydrogen bonds involve fluorine atoms only, despite the presence of an oxygen atom that could serve as an acceptor (see Table S3 in the Supporting Information).

Because of the small difference in electronegativity between C and H atoms, in both PMCB and TDCB the hydrogen bonds are expected to be weak. Although it was demonstrated that

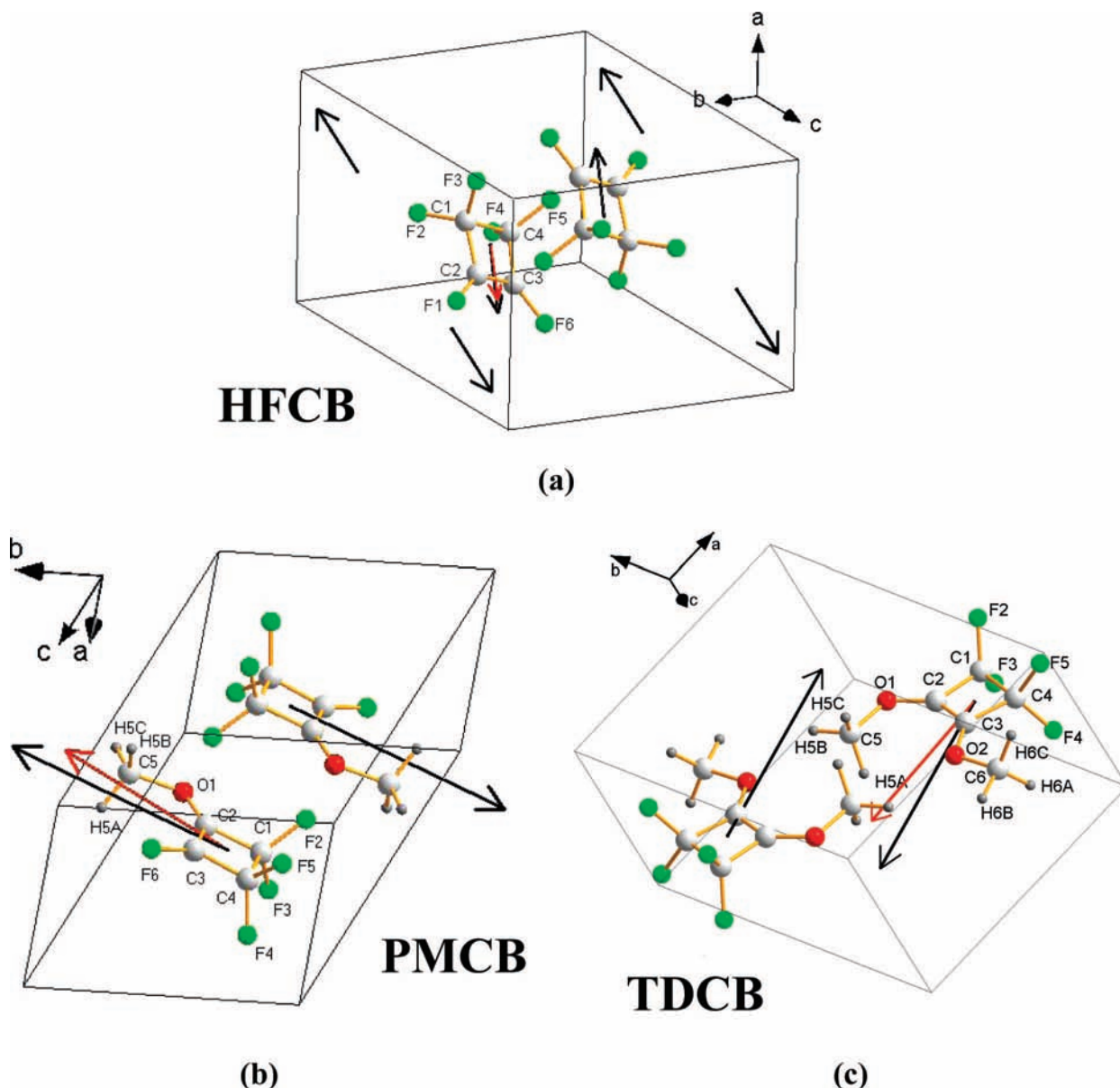


Figure 4. Dipole motifs of HFCB, PMCB, and TDCB in their respective unit cells. Dipole moments are shown as calculated from the QTAIM partitioning of the primary density with the molecular center of mass as their point of application. Black arrows: solid-state optimized geometry at the B3LYP/6-31G(d) theory level. Red arrows: gas-phase optimized geometry at the B3LYP/6-311+Gd theory level. Ball-and-stick pictures created by Diamond v3.1f (Brandenburg, K. *Diamond-Crystal and Molecular Structure Visualization*; Crystal Impact GbR: Bonn, Germany, 2008; <http://www.crystalimpact.com/diamond>).

C–H \cdots O interactions of comparable strength as the O–H \cdots O ones can exist in organic molecules,⁴⁹ this is not the case for our fluorocyclobutene methoxy derivatives. Looking at Tables S3 and S5 in the Supporting Information, it is clear that all the hydrogen bonds are quite long [neither in PMCB nor in TDCB are such H–bonds shorter than 2.5 Å, with the only exceptions being C5–H5C \cdots F5 (2.4038 Å) and C5–H5A \cdots F3 (2.4976 Å) occurring in pairs A and B of TDCB] and some of them are characterized by very narrow H-bond angles (as an example, C5–H5C \cdots O2 in pair L of TDCB has a bond angle of 100.7°). Moreover, their electron densities at the bcp's are small, with 0.054 e Å⁻³ as the greatest value occurring at the C5–H5C \cdots F5 bcp in pair A of TDCB.

It is worth noting that in these systems hydrogen atoms seem to prefer the interaction with fluorine rather than with oxygen atoms. From a statistical point of view, in PMCB the five fluorine atoms constitute 83% of the available hydrogen-bond acceptors, while the only oxygen atom covers the remaining

17%. Yet, no H \cdots O intermolecular bcp's have been found. All the interactions involving the vinylic substituents seem to prefer F6 as a hydrogen-bond acceptor (see Figure SF2 in the Supporting Information, pairs D and H). In TDCB the oxygen percentage against the total number of available acceptors doubles to 33% and four C–H \cdots O hydrogen bonds are formed, that is, 31% of the total number of symmetry-independent hydrogen bonds. Nevertheless, these C–H \cdots O interactions are very long (with bond lengths over 2.7 Å), and the electron density at their bcp's is lower than that at the bcp's of most C–H \cdots F interactions (see Table S5 in Supporting Information).

4.5. Crystal Energies. Table 6 reports the crystal cohesive energies of HFCB, PMCB, and TDCB, corrected for BSSE,^{23,37} as evaluated from single-point B3LYP/DZ^{25,36} periodic calculations at the optimized geometries in the solid-state. As expected, the relaxation energy provides a minor contribution for all these systems. More interestingly, we observe that the total corrected crystal cohesive energy is unrealistically calculated as small and

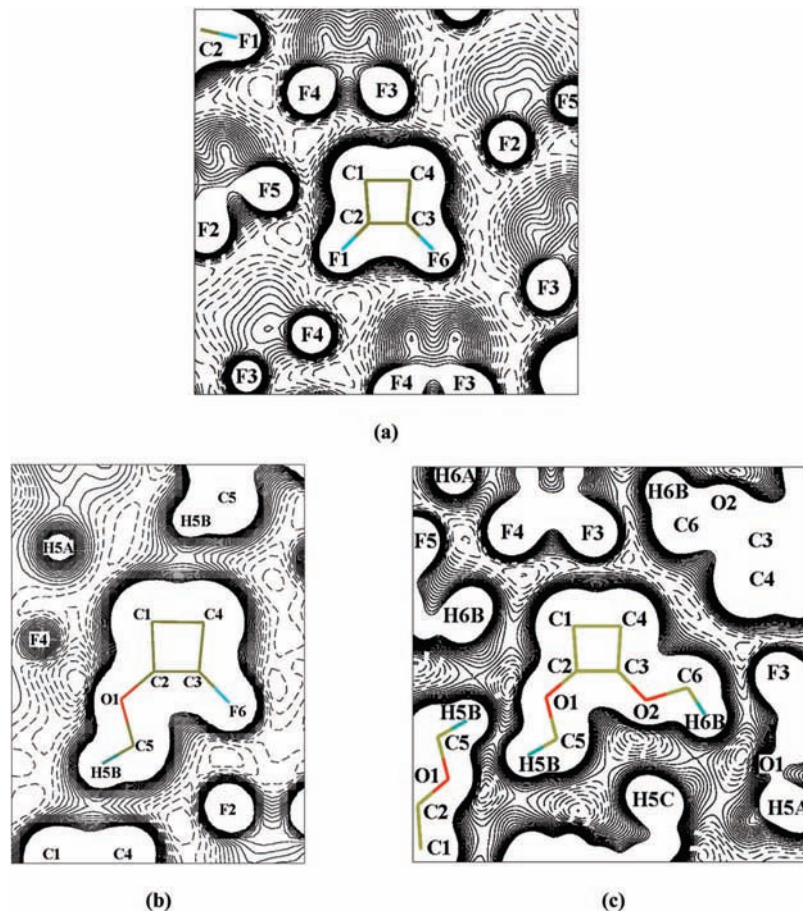


Figure 5. Electrostatic potential in the main molecular plane (cyclobutene ring) as evaluated from the periodic primary density of HFCB, PMCB, and TDCB. Molecular wireframes are superimposed. All the atoms within 1.0 Å from the reference plane are labeled (see Scheme 2). Level lines range within ± 0.1 au with a step of 0.0065 au (corresponding roughly to ± 0.2 e Å⁻¹, with a step of 0.01 e Å⁻¹). Dashed lines, negative contours; full lines, positive contours. 1.0 Å corresponds approximately to 1 cm on the maps. (a) C₄F₆, HFCB; (b) C₄F₅OCH₃, PMCB; and (c) C₄F₄(OCH₃)₂, TDCB.

positive for all three substances. This is likely to be the consequence of lacking the dispersive term in the DFT Hamiltonian (see Computational Details above). So, in spite of hydrogen bonds, and notwithstanding the enhancement of the molecular dipole moments, the dispersive term to the total energy appears to be essential, even in PMCB and TDCB. Because within this energy decomposition scheme it is impossible to make hypotheses on the importance of the dispersion energy, it is hard to discriminate the effect of this term on the stability of the PMCB and TDCB crystals with respect to HFCB. To gain a deeper insight into the contributions to the total cohesive energy, the Spackman's E_{cryst} model^{40–44} was applied to an atom-centered Mulliken spherical-harmonics multipole expansion of $\rho(\mathbf{r})$ up to $l = 4$ (see also the Supporting Information). Table 7 shows such contributions for the three substances within the E_{cryst} scheme.

As expected on the basis of the increase of the melting point along the series HFCB–PCMB–TDCB (Table 1), the total energy appears to be more negative for TDCB and PMCB with respect to HFCB. Spackman's model predicts E_{cryst} to be dominated by the dispersion energy in all three substances: in HFCB, the latter term provides 76% of the total attractive energy ($E_{\text{dis}} + E_{\text{el}}$), while its contribution is 71% in PMCB and 67% in TDCB. This is in agreement with the fact that although it is possible that an observed crystal packing could be the consequence of strong electrostatic dipolar interactions (as in the case of diphenyl ethers⁵⁶), the dipole–dipole interaction does not always give the major contribution to the total crystal stabiliza-

TABLE 6: Crystal Cohesive Energies of HFCB, PMCB, and TDCB As Evaluated Directly from Periodic Wave Functions with the B3LYP/DZ (Dunning) Theory Level at the Optimized Geometry in the Solid State (see the text)^a

	HFCB	PCMB	TDCB
crystal binding energy per molecule ^b	−13.19	−19.47	−22.67
relaxation energy per molecule ^c	−0.60	−1.71	−1.23
total cohesive energy per molecule ^d	−12.59	−17.76	−21.44
total crystal cohesive energy ^e	−50.36	−35.52	−42.89
BSSE correction ^f	24.27	25.03	25.28
total cohesive energy per molecule, BSSE corrected	11.68	7.27	3.83
total crystal cohesive energy, BSSE corrected	46.73	14.54	7.67

^a All values are given in kJ/mol. ^b Defined as the difference between the energy per molecule in the solid state less its gas-phase energy in the same geometry as in the crystal. ^c Calculated with Gaussian 03, using the standard 6-311+G(d) basis set with the DFT B3LYP Hamiltonian. The relaxation energy is defined as the difference in the gas-phase energy between the molecular relaxed geometry and its solid-state geometry. ^d Defined as the crystal binding energy per molecule plus the relaxation energy. ^e Defined as the energy difference between the total unit cell energy and the same energy evaluated for an ideal crystal made of noninteracting molecules. The relaxation energy contribution is also added for each molecule. ^f Evaluated with the counterpoise (CP) method, taking into account all the “ghost” atoms within 5.0 Å from the molecule (see the text).

TABLE 7: Comparison between Various Contribution to the Intermolecular Interaction Energies As Evaluated by Spackman's E_{cryst} Model Applied to the Mulliken Distributed Multipole Analysis of the B3LYP/DZ (Dunning) Periodic Electron Density at the Solid-State Optimized Geometry^a

	HFCB	PMCB	TDCB
total E_{cryst} energy	-50.97	-58.21	-62.33
repulsion energy	37.86	48.22	68.59
dispersion energy ^b	-67.90	-75.65	-88.17
electrostatic energy	-20.93	-30.78	-42.75
$E_{\text{pro-pro}}$	-14.22	-18.29	-27.62
$E_{\text{pro-def}}$	-0.32	-0.24	0.14
$E_{\text{def-def}}$	-6.39	-12.25	-15.27

^a All values are given in kJ/mol. ^b Scaled with the dampening function proposed by Grimme. See the text.

tion, and sometimes its role appears negligible.^{57,58} In the present investigation, the dispersion energy is the most significant term. Anyway, the electrostatic interactions are known to be important in crystals,^{59,60} and as a matter of fact, even in HFCB they are not neglected, as would be the case for totally nonpolar molecules (e.g., the series of *n*-alkanes with increasing molecular mass). The reduction of the calculated density in the solid phases in the HFCB–PMCB–TDCB series (see Table 1) is likely the consequence of the occurrence of other interactions besides the dispersive ones (e.g., Coulombic interactions and hydrogen bonds). In fact, if the only significant contribution to the total energy along a series of homologous compounds were the van der Waals term, the density would be expected to increase monotonically with the molecular mass (as in the well-known case of the *n*-alkanes).

Interestingly, the promolecule–promolecule contribution ($E_{\text{pro-pro}}$) to E_{el} is the leading term for all three substances, although the multipole contribution ($E_{\text{def-def}}$) gradually increases from HFCB to TDCB.

5. Summary and Conclusions

(a) The geometries of hexafluorocyclobutene and its vinyl methoxy derivatives were here optimized for the first time by means of a periodic calculation at the DFT-B3LYP/6-31G(d) level. For the perfluorinated compound, our results agree qualitatively with accurate CCSD(T)/cc-pVTZ calculations in the gas phase reported by Császár, with bond lengths that appear slightly overestimated. A possible explanation of this discrepancy has been offered in the Supporting Information. In spite of its well-recognized limits when used to optimize gas-phase geometries, the DFT-B3LYP Hamiltonian should be considered as a reliable compromise between the speed of calculation and its accuracy, when applied to optimizations in the solid state. A basis set larger than 6-31G(d) could reduce the overestimate of some bond lengths in C_4F_6 , which in the current work are longer with respect to both the experimental and theoretical results reported in the literature (see Table 2).

(b) A full topological analysis of the total, solid-state charge densities according to QTAIM, together with the evaluation of electrostatic properties and cohesive energies, was carried out to investigate the effect of the vinyl methoxy substituents on the electronic properties and crystal packing of the fluorinated cyclobutenes.

As regards the effect of the OCH_3 substituents on the electronic properties of the four-membered carbon ring, it was found that the insertion of the first methoxy group causes the major axis (λ_2) eigenvectors of the Hessian of $\rho(\mathbf{r})$ at O1-C2 , C2=C3 , C1-C2 , C4-C3 , and C3-F6 bcp's to align almost

perfectly to each other. Simultaneously, the C3-F6 bond weakens, in that it lengthens by about 1% and loses as much as 4% of its charge density at the bcp. This electronic rearrangement could be interpreted by means of the electron-withdrawing ability of the equatorial F6, which attracts the charge density provided by the methoxy donor group through the delocalized π system around the C2=C3 bond. The increment in the electronic population in the atomic basin of C3 also increases the Coulombic repulsion with the adjacent F6 basin, resulting in a new equilibrium distance that is slightly increased with respect to that found in the parent compound C_4F_6 . Analogous geometry changes were detected by comparing bond distances in *cis*-1,2-difluoroethylene and *cis*-1-fluoro-2-methoxyethylene in the gas phase at both B3LYP/6-31G(d) and CCSD/TZ levels of theory. When the second OCH_3 group is added to the cyclobutene ring, a more symmetrical charge distribution appears around the vinyl bond, in that the net charges of the C2/C3 and O1/O2 basins, as well as the electron density and its Laplacian at the corresponding bcp's, became similar to each other.

As regards the crystal packing, the dispersion contribution to the total crystal cohesive energy was proven to be the leading term for all three cyclobutenes. A significant enhancement of the modulus of the dipole moment was detected upon substitution, as large as 202% ($\text{C}_4\text{F}_6\text{-C}_4\text{F}_5\text{OCH}_3$) and 235–236% ($\text{C}_4\text{F}_6\text{-C}_4\text{F}_4(\text{OCH}_3)_2$); this in turn provides a considerable contribution to the electrostatic part of the crystal energy. The hydrogen bonds are all long and weak, being characterized by very small $\rho(\mathbf{r})_{\text{bcp}}$ values. The present results indicate some preference for the $\text{H}\cdots\text{F}$ interactions with respect to the $\text{H}\cdots\text{O}$ ones in substituted fluorinated cyclobutenes.

A concluding remark appears to be noteworthy. It was a very difficult task to obtain even polycrystalline samples of the perfluorinated compound and its methoxy derivatives. The quality of the XRD results is satisfactory as regards the *R* indices and the accuracy of the final molecular parameters, but the latter were not sufficient in terms of precision to be used by themselves for the accurate electron density determination. Therefore, in order to compare homogeneous results, and at the same time to get rid of the spurious effects due to the sample quality, full periodic geometry optimizations were mandatory for all three substances. It is important anyway to stress that the XRD results constituted an essential, physically reliable starting point, not otherwise available, to perform all the subsequent periodic optimizations. So, this study should be considered as a further example of the power of joint experimental and theoretical methods in dealing with electronic effects in solids.

Acknowledgment. Thanks are due to Dr. Mario Barzaghi (CNR-ISTM, Milano, Italy) for thoughtful discussions and for his precious help with the PAMoC code. The authors wish to acknowledge also Dr. Bartolomeo Civalleri (University of Torino, Torino, Italy) for useful comments. This work was supported by Italian MIUR (Fondi FIRST-Unimi 2007–2008).

Supporting Information Available: Description of the crystallization procedure. Details on the computational method employed for the periodic optimization. Details on the topological analysis. Details on the E_{cryst} model for the crystal energy evaluation. Comparison of geometry optimization results for HFCB in the solid state with those reported in ref 10 on the isolated molecule. Full list of the noticeable critical points of the electron density in the asymmetric unit for all three derivatives. Geometry of hydrogen bonds and corresponding topological parameters. For all three substances, a ball-and-stick

representation of the molecular pairs at increasing center of mass distances, with the intermolecular bond critical point positions highlighted. This material is available free of charge via the Internet at <http://pubs.acs.org>.

References and Notes

- Barthel-Rosa, L. P.; Gladysz, J. A. *Coord. Chem. Rev.* **1999**, *190*–192, 587.
- Patani, G. A.; LaVoie, E. J. *Chem. Rev.* **1996**, *96*, 3147.
- Zhao, K.; Lim, D. S.; Funaki, T.; Welch, J. T. *Bioorg. Med. Chem.* **2003**, *11*, 207.
- Muller, K.; Fach, C.; Diederich, F. *Science* **2007**, *317*, 1881.
- Timperley, C. M. *J. Flourine Chem.* **2004**, *125*, 685.
- Sievert, A. C.; Nappa, M. J.; Minor, B. H.; Leck, T. J.; Rao, V. N. M.; Swearingen, E. N.; Schmitt, C.; Mouli, N.; Perti, D. *PCT Int. Appl. WO 2006-US42686 20061031*, 2007, 133 pp.
- Terasaki, A.; Seki, J.; Tanaka, I. *U.S. Pat. Appl. Publ.* **2007**, 18 pp, Patent Application US 2006–606874 20061201.
- Yu, J. S.; Kim, J.-K. *U.S. Pat. Appl. Publ.* **2007**, 11 pp, Patent Application US 2006–479287 20060629.
- Hertwig, R. H.; Koch, W.; Maksic, Z. B. *J. Phys. Chem.* **1995**, *99*, 173.
- Császár, A. G. *J. Phys. Chem. A* **2004**, *108*, 2002.
- Han, Y.-K.; Lee, Y. S.; Lee, S. Y.; Kim, J. T. *J. Mol. Struct. (Theochem)* **1998**, *422*, 25.
- Shiotani, M.; Persson, P.; Lunell, S.; Lund, A.; Williams, F. J. *Phys. Chem. A* **2006**, *110*, 6307.
- Császár, A. G.; Hedberg, K. *J. Phys. Chem.* **1990**, *94*, 3525.
- Hedberg, L.; Hedberg, K. *J. Phys. Chem.* **1993**, *97*, 10349.
- Xu, L. W.; Klausner, M. E.; Andrews, A. M.; Kuczowski, R. L. *J. Phys. Chem.* **1993**, *97*, 10346.
- Bader, R. F. W. *Atoms in Molecules: A Quantum Theory*; Oxford University Press: Oxford, 1990.
- Gatti, C. Z. *Kristallogr.* **2005**, *220*, 399.
- Smart, B. E.; Reddy, G. S. *J. Am. Chem. Soc.* **1976**, *98*, 5596.
- Lunelli, B. *Inorg. Chim. Acta* **2007**, *360*, 1217.
- SMART1000 User Manual; Bruker AXS Inc.: Madison, WI, 2001.
- Sheldrick, G. M. *Acta Crystallogr.* **2008**, *A64*, 112–122.
- CCDC 708295–708297 contains the supplementary crystallographic data for this paper. These data can be obtained free of charge from The Cambridge Crystallographic Data Centre via www.ccdc.cam.ac.uk/data_request/cif.
- Saunders, V. R.; Dovesi, R.; Roetti, C.; Orlando, R.; Zicovich-Wilson, C. M.; Harrison, N. M.; Doll, K.; Civalleri, B.; Bush, I. J.; D'Arco, Ph.; Llunell, M. *CRYSTAL2003 User's Manual*; University of Torino, Torino, 2003.
- Franch, M. M.; Petro, W. J.; Hehre, W. J.; Binkley, J. S.; Gordon, M. S.; DeFrees, D. J.; Pople, J. A. *J. Chem. Phys.* **1982**, *77*, 3654.
- Basis sets were obtained from the Extensible Computational Chemistry Environment Basis Set Database, Version 02/02/06, as developed and distributed by the Molecular Science Computing Facility, Environmental and Molecular Sciences Laboratory, which is part of the Pacific Northwest Laboratory, P.O. Box 999, Richland, Washington 99352, and funded by the U.S. Department of Energy. The Pacific Northwest Laboratory is a multiprogram laboratory operated by Battelle Memorial Institute for the U.S. Department of Energy under contract DE-AC06-76RLO 1830. See also <https://bse.pnl.gov/bse/portal>.
- Becke, A. D. *J. Chem. Phys.* **1993**, *98*, 5648.
- Lee, C.; Yang, W.; Parr, R. G. *Phys. Rev. B* **1988**, *37*, 785.
- Frisch, M. J.; Trucks, G. W.; Schlegel, H. B.; Scuseria, G. E.; Robb, M. A.; Cheeseman, J. R.; Montgomery, J. A., Jr.; Vreven, T.; Kudin, K. N.; Burant, J. C.; Millam, J. M.; Iyengar, S. S.; Tomasi, J.; Barone, V.; Mennucci, B.; Cossi, M.; Scalmani, G.; Rega, N.; Persson, G. A.; Nakatsuji, H.; Hada, M.; Ehara, M.; Toyota, K.; Fukuda, R.; Hasegawa, J.; Ishida, M.; Nakajima, T.; Honda, Y.; Kitao, O.; Nakai, H.; Klene, M.; Li, X.; Knox, J. E.; Hratchian, H. P.; Cross, J. B.; Bakken, V.; Adamo, C.; Jaramillo, J.; Gomperts, R.; Stratmann, R. E.; Yazyev, O.; Austin, A. J.; Cammi, R.; Pomelli, C.; Ochterski, J. W.; Ayala, P. Y.; Morokuma, K.; Voth, G. A.; Salvador, P.; Dannenberg, J. J.; Zakrzewski, V. G.; Dapprich, S.; Daniels, A. D.; Strain, M. C.; Farkas, O.; Malick, D. K.; Rabuck, A. D.; Raghavachari, K.; Foresman, J. B.; Ortiz, J. V.; Cui, Q.; Baboul, A. G.; Clifford, S.; Cioslowski, J.; Stefanov, B. B.; Liu, G.; Liashenko, A.; Piskorz, P.; Komaromi, I.; Martin, R. L.; Fox, D. J.; Keith, T.; Al-Laham, M. A.; Peng, C. Y.; Nanayakkara, A.; Challacombe, M.; Gill, P. M. W.; Johnson, B.; Chen, W.; Wong, M. W.; Gonzalez, C.; Pople, J. A. *Gaussian 03, revision C.02*; Gaussian, Inc.: Wallingford, CT, 2004.
- Only in the case of PMCB (which has an intermediate number of atoms between HFBC and TDCB) was a full frequency analysis performed with the CRYSTAL06 program, as this version of the code allows the evaluation of the vibration modes in the condensed phase at the G point. The calculation took about 3 weeks on a very powerful computing platform with a 3056 MHz CPU. As expected, only the first three modes (i.e. those corresponding to the lowest frequencies) showed very small ($\sim 10^{-9}$) and negative eigenvalues. Actually, the latter should be zero at the G point, as they correspond to the translational (acoustic) degrees of freedom of the molecule as a whole. No other negative eigenvalue has been found, confirming that the optimized solid-state geometry of PMCB corresponds to a true minimum on the PES.
- Krishnan, R.; Binkley, J. S.; Seeger, R.; Pople, J. A. *J. Chem. Phys.* **1980**, *72*, 650.
- For the gas-phase calculations, we also checked the 6-31G(d) basis set, which is the same used in the periodic optimizations, with the same DFT B3LYP Hamiltonian. Qualitatively, we obtained the same results as in the 6-311+G(d) calculations; anyhow, a larger basis set with diffuse functions on C and F atoms is essential to properly describe the electrostatic properties and the relaxation energies of the isolated molecules. The Mulliken dipole vector modulus, as an example, is equal to 1.289, 4.274, and 4.377 D in HFBC, PMCB, and TDCB optimized gas-phase geometries at the 6-31G(d) theory level, respectively. The introduction of the diffuse functions on the heavy atoms (6-31+G(d) basis set) increases the same quantities to 1.476, 4.600, and 5.210 D, respectively. When the larger 6-311+G(d) basis set is used, a further (although much smaller) increment of the vector moduli takes place, their values becoming 1.556, 4.680, and 5.283 D, respectively. Additional introduction of diffuse functions (6-311++G(d) basis set) or polarization functions (6-311+G(d,p) basis set) on the hydrogen atoms in the two methoxy derivatives has a negligible influence on both their dipole vectors and their relaxation energies. We therefore chose the 6-311+G(d) basis set as our reference theory level for all the present gas-phase optimizations.
- Saunders, V. R.; Dovesi, R.; Roetti, C.; Causà, M.; Harrison, N. M.; Orlando, R.; Zicovich-Wilson, C. M. *CRYSTAL98 User's Manual*; University of Torino: Torino, Italy, 1999.
- Gatti, C. *TOPOND 98 User's Manual*; CNR-ISTM: Milano, Italy, 1999.
- The residual charge is defined as the difference between the molecular charge obtained by summing the electron population in each atomic basin and the true molecular charge (zero, in the present case). It should be considered as an index of the integration accuracy.
- Civalleri, B.; Doll, K.; Zicovich-Wilson, C. M. *J. Phys. Chem. B* **2007**, *111*, 26.
- Dunning, T. H., Jr.; Hay, P. J. *Methods of Electronic Structure Theory*; Schaefer H. F., III, Ed.; Plenum Press: New York, 1977; Vol. 3.
- Boys, S. F.; Bernardi, F. *Mol. Phys.* **1970**, *19*, 553.
- van Mourik, T.; Gdanitz, R. J. *J. Chem. Phys.* **2002**, *116*, 9620.
- Dobson, J. F.; McLennan, K.; Rubio, A.; Wang, J.; Gould, T.; Lee, H. M.; Dinte, B. P. *Aust. J. Chem.* **2001**, *54*, 523.
- Spackman, M. A. *J. Phys. Chem.* **1987**, *91*, 3179.
- Spackman, M. A. *J. Chem. Phys.* **1986**, *85*, 6587.
- Spackman, M. A. *J. Chem. Phys.* **1986**, *85*, 6579.
- Spackman, M. A.; Weber, H. P.; Craven, B. M. *J. Am. Chem. Soc.* **1988**, *110*, 775.
- Spackman, M. A. Keynote Lecture KN23.28 at IUCR2005, Book of Abstracts; Firenze; 2005; p C5.
- Barzaghi, M. *PAMoC (Version 2002.0), Online User's Manual*; CNR-ISTM, Institute of Molecular Science and Technologies: Milano, Italy, 2002; URL: www.istm.cnr.it/~barz/pamoc/.
- Grimme, S. *J. Comput. Chem.* **2006**, *27*, 1787.
- Bianchi, R.; Forni, A.; Oberti, R. *Phys. Chem. Minerals* **2005**, *32*, 638.
- Roversi, P.; Barzaghi, M.; Merati, F.; Destro, R. *Can. J. Chem.* **1996**, *74*, 1145.
- Lo Presti, L.; Soave, R.; Destro, R. *J. Phys. Chem. B* **2006**, *110*, 6405.
- Shriver, D. F.; Atkins, P. W.; Langford, C. H. *Inorg. Chem.*, 2nd ed.; Oxford University Press: Oxford, 1994; p 42.
- Brahms, D. L. S.; Dailey, W. P. *Chem. Rev.* **1996**, *96*, 1585.
- Feller, D. J. *J. Comput. Chem.* **1996**, *17*, 1571.
- Schuchardt, K. L.; Didier, B. T.; Elsethagen, T.; Sun, L.; Gurmooorthi, V.; Chase, J.; Li, J.; Windus, T. L. *J. Chem. Inf. Model.* **2007**, *47*, 1045.
- Dunning, T. H. *J. Chem. Phys.* **1971**, *55*, 716–723.
- Spackman, M. A. *Chem. Rev.* **1992**, *92*, 1769.
- Dey, A.; Desiraju, G. R. *Chem. Commun.* **2005**, 2486.
- Gavezzotti, A. *J. Phys. Chem.* **1990**, *94*, 4319.
- Whitesell, J. K.; Davis, R. E.; Saunders, L. L.; Wilson, R. J.; Feagins, J. P. *J. Phys. D: Appl. Phys.* **1993**, *26*, B56.
- Tsirelson, V. G.; Ozerov, R. P. *Electron Density and Bonding in Crystals*; Institute of Physics Publishing: Philadelphia, 1996; Chapter 7.1.2, p 368.
- Suponitsky, K. Y.; Tsirelson, V. G.; Feil, D. *Acta Crystallogr.* **1999**, *A55*, 821.
- Park, J. D.; Sharrah, M. L.; Lacher, J. R. *J. Am. Chem. Soc.* **1949**, *71*, 2337.